



# Experimental investigation of nanofluid stability on thermal performance and flow regimes in pulsating heat pipe

Ali Akbari<sup>1</sup> · Mohammad Hassan Saidi<sup>1</sup>

Received: 8 February 2018 / Accepted: 17 May 2018 / Published online: 25 May 2018  
© Akadémiai Kiadó, Budapest, Hungary 2018

## Abstract

Pulsating heat pipe (PHP) is a type of wickless heat pipe that has a simple structure and an outstanding thermal performance. Nanofluid is a type of fluid in which nanoparticles are dispersed in a base fluid and have generally a better thermal conductivity in comparison with its base fluid. In this article, the performance of a nanofluid PHP is investigated. Graphene/water nanofluid with a concentration of 1 mg mL<sup>-1</sup> and TiO<sub>2</sub> (titania)/water nanofluid with a concentration of 10 mg mL<sup>-1</sup> are used as the working fluids. To simultaneously investigate the thermal performance and flow regimes in the PHP, a one-turn copper PHP with a Pyrex glass attached to its adiabatic section is used. A one-turn Pyrex PHP is also used to fully visualize flow patterns in the PHP. Our results show that the material for the fabrication of a PHP and temperature of the working fluid are the most important parameters that affect the stability of a nanofluid in the PHP. The more stable nanofluid keeps its stability in the copper PHP, while the less stable nanofluid starts to aggregate right after the injection to the copper PHP. The more stable nanofluid has a better thermal performance than water, while the less stable nanofluid has a worse thermal performance than water. In the case of flow regimes, no significant differences are observed between the nanofluid PHP and the water PHP which is different from the previous observations. These results can help researchers to choose the best working fluid for PHPs.

**Keywords** Pulsating heat pipe (PHP) · Titania/water nanofluid · Graphene/water nanofluid · Flow patterns/regimes · Thermal performance

## List of symbols

$A$  Surface area (m<sup>2</sup>)  
 $h$  Heat transfer coefficient (W m<sup>-2</sup> °C<sup>-1</sup>)  
 $L$  Length (m)  
 $Q$  Heat input (W)  
 $R$  Thermal resistance (°C W<sup>-1</sup>)  
 $r$  Radius (m)  
 $T$  Temperature (°C)

## Greek letters

$\delta$  Differential operator

## Subscripts

cond Condenser  
Eff Effective  
evp Evaporator  
log Data logger

## Introduction

Pulsating heat pipe (PHP) was first introduced by Akachi [1] in 1990. It has three sections: evaporator, condenser, and adiabatic section; where in the evaporator section, heat is applied to the device, in the condenser section, heat is removed from it by a coolant, and the adiabatic section stands between these two sections and has no heat transfer with the surroundings. Heat transfer mechanisms in the PHP are nucleation and growth of bubbles in the evaporator and shrinkage and collapse of them in the condenser. Several experiments have already been conducted and the effects of several parameters such as number of turns, type of working fluid, filling ratio (FR), inclination angle, and

✉ Mohammad Hassan Saidi  
saman@sharif.edu

Ali Akbari  
ali\_akbari@mech.sharif.edu

<sup>1</sup> Center of Excellence in Energy Conversion (CEEC), School of Mechanical Engineering, Sharif University of Technology, P.O. Box 11155-9567, Tehran, Iran

heat input on the thermal performance and flow regimes in PHPs have been investigated.

In a nanofluid, nanoparticles are dispersed homogeneously in the base fluid. Because of the high thermal conductivity of the nanoparticles, larger surface-to-volume ratio of the nanoparticles, and the Brownian motion of the nanoparticles in the base fluid, the nanofluid has a higher thermal conductivity than the base fluid. The higher thermal conductivity of the nanofluid enhances the sensible portion of the heat transfer in the PHP and improves its thermal performance. Although nanofluids are good choices for heat transfer applications, they have some disadvantages. Their viscosity is higher than the base fluid and nanoparticles can erode the channel that the nanofluid flows inside it. Nanofluids have been investigated both numerically and experimentally. Nasiri et al. [2] investigated nanofluidic flow around a horizontal cylinder numerically. They did their simulations using weakly compressible smoothed particle hydrodynamics (WCSPH). Their results showed that the heat transfer characteristics of the flow when the working fluid was nanofluid were better than the case with the base fluid. The improvement was more obvious when Reynolds number and particle volume concentration increased. Safaei et al. [3] studied the performance of graphene nanoplatelet (GNP)/silver water-based nanofluids streaming in a rectangular channel. Their results showed that there is a concentration of nanosheets in the nanofluid which improves heat transfer compare to the base fluid. In addition, increasing the concentration leads to an increase in the friction factor, pressure drop, and pumping power. Safaei et al. [4] did a survey on experimental and numerical investigations in the field of nanofluid heat transfer. They stated that most of the numerical works declared an enhancement in heat transfer characteristics using nanofluids, although some experimental works are reporting that nanofluids worsen heat transfer. They argue that in the experiments,  $\text{Al}_2\text{O}_3/\text{water}$  and  $\text{titania}/\text{water}$  more often are used as nanofluid. Therefore, benchmark experiments are not comprehensive to verify numerical results. Safaei et al. [5] numerically investigated the fluid flow and heat transfer of  $\text{Cu}/\text{water}$  nanofluid inside a 2D rectangular ribbed microchannel. For the simulation, they used a Reynolds number of 50, Richardson numbers between 0.1 and 10, nanoparticles volume fractions of 0.0–0.04, and inclination angles in the range of  $0^\circ$ – $90^\circ$ . Their results showed that with increasing the inclination angle or volume fraction of nanoparticles, heat transfer and pressure drop increase. Heydari et al. [6] did a similar simulation. They studied the effect of attack angle of triangular ribs, volume fraction of nanoparticles, nanoparticles diameter, and Reynolds number on heat transfer in a microchannel. They used  $\text{Ag}/\text{water}$  nanofluid as the cooling fluid. Their results represented that using nanofluids containing nanoparticles with smaller

diameters improves heat transfer rate. However, the diameter of nanoparticles has no effect on the friction coefficient and pumping power. Safaei et al. [7] did a numerical investigation on the erosion of  $\text{Cu}/\text{water}$  micro- and nanofluid that flow inside a  $90^\circ$  elbow. They concluded that the rate of erosion increases with particle diameter, volume fraction of nanoparticles, and inlet flow velocity. Karimpour et al. [8] studied laminar mixed convection of  $\text{Cu}/\text{water}$  nanofluid in an inclined lid driven cavity using lattice Boltzmann method. They found out that in all states, the larger volume fraction of nanoparticles leads to a larger Nusselt number. Karimpour et al. [9] investigated laminar forced convection of  $\text{Cu}/\text{water}$  nanofluid in a microchannel using lattice Boltzmann method. Their results showed that increasing volume fraction of nanoparticles causes an increase in Nusselt number. Raei et al. [10] conducted an experimental investigation to study the effects of  $\text{Al}_2\text{O}_3/\text{water}$  nanofluid on the hydrodynamics and convective heat transfer of a counter flow double-tube heat exchanger. Their results showed that nanofluids have a higher Nusselt number than pure water. Stalin et al. [11] performed the theoretical and experimental analysis for a flat-plate solar collector operating with water and  $\text{CeO}_2/\text{water}$  nanofluid as the working fluids. They observed while using nanofluid as the working fluid, the maximum efficiency of solar water heater was 21.5% higher comparing to the case in which water was used as the base fluid.

There are a large number of studies on the effect of nanofluid on the thermal performance of PHPs. Several researchers have observed improvements in PHP performance using nanofluids [12–17], while some have reported a deterioration of it [18, 19]. Having the same performance as the conventional fluid is another observation which has been reported when nanofluid is used as the working fluid in a PHP [20].

The diversity in the observations is due to the complicated operating mechanism of a nanofluid PHP. When heat is applied to a PHP, the nanofluid becomes unstable and the aggregation of nanoparticles begins. The agglomerated nanoparticles settle on the surface of the PHP, changing the surface roughness of it as a result. Surface roughness is an important subject in PHP operation. Variations in surface roughness directly affect the nucleation process. Precipitated nanoparticles can change surface roughness in a way that the number of nucleation sites increases, decreases, or does not change. Knowing this, the diversity in the observations and results of the nanofluid PHP can be justified. When the precipitation causes an increase in the number of nucleation sites, it leads to an earlier startup and nucleation of the bubbles. On the other hand, when the precipitation causes a decrease in the number of nucleation sites, the startup process disrupts, and the thermal performance deteriorates.

As heat input increases, and so, temperature of the working fluid rises, the motion of nanoparticles in the base fluid becomes faster. This faster motion causes more collisions between the nanoparticles, and the agglomeration becomes more intense. Finally, the nanofluid turns to the base fluid and there will not be any nanoparticles in the base fluid any longer. Das et al. [21] claimed that the thermal conductivity of a nanofluid is a function of temperature and thermal conductivity increases with it as well. Esfe et al. [22] reported the increase of thermal conductivity of DWCNT-ZnO/water–ethylene glycol nanofluids with increasing temperature of the nanofluid and volume fraction of the nanoparticles. In addition, they stated that the effect of volume fraction of nanoparticles is more significant than the effect of temperature. Hence, if there is a stable nanofluid at high heat inputs, improved thermal performance of PHP can be expected.

Therefore, nanofluids can influence PHP performance in two ways: (1) increase in the thermal conductivity of the working fluid that leads to an increase in the sensible portion of heat transfer and (2) the agglomeration and sedimentation of the nanoparticles that can change the number of nucleation sites. To the best of our knowledge, in all the previous works, changes in surface roughness have been random and there have been no control on the process of sedimentation. In most of the previous studies, these mechanisms affect the thermal performance of PHP and the dominant mechanism has not been cleared. When nanoparticles precipitate on the surface of the evaporator, nanofluid turns to the base fluid and its thermal conductivity is not high anymore. Having two nanofluids with different levels of stability, the dominant mechanism can be discussed with a more accuracy and the effect of thermal conductivity will be observed better.

The observations on the effect of nanofluids on flow regimes are also diverse. Wilson et al. [23] reported that they did not observe any nucleation in their nanofluid PHP. Neutron radiography was their method to visualize the flow in the PHP and they mentioned that the temporal and spatial obstacles of the neutron-imaging detector may be one reason that no nucleation was observed. Bhuwakietkumjohn and Rittidech [24] did the visualization through a closed-loop PHP that had two check valves and was made of Pyrex glass. They reported that with increasing the evaporator temperature, the flow regime changes from annular flow along with slug flow to slug flow along with bubble flow and then to dispersed bubble flow along with bubble flow. This sequence is the same for both the ethanol PHP and the silver/ethanol nanofluid PHP. However, the heat flux is higher for the nanofluid PHP. Li et al. [25] investigated the flow regimes in a PHP made of quartz glass when it was filled with DI water and SiO<sub>2</sub>/DI water nanofluid. In the water PHP, the only regime they observed was column flow. However, in the nanofluid

PHP, column flow, slug flow, and annular flow were observed. In addition, they reported that the dryout heat load for the nanofluid PHP was 2–3 times greater than the dryout heat load for the water PHP. This is due to the fact that nucleation boiling occurs more easily in the nanofluid PHP. Ji et al. [20] used a PDMS PHP to visualize flow regimes. Their working fluids were ethanol and Al<sub>2</sub>O<sub>3</sub>/ethanol nanofluid. They reported that there was no difference between the thermal performances of the ethanol PHP and the nanofluid PHP. When the working fluid was nanofluid, the sedimentation of nanoparticles and the nucleation of a large number of small bubbles were observed. Goshayeshi and Chaer [26] reported the results of visualization of a Pyrex PHP. They used Fe<sub>2</sub>O<sub>3</sub>/kerosene nanofluid as the working fluid. In synthesizing the nanofluid, oleic acid was used as the surfactant. The flow regimes they observed in the PHP were bubble flow, slug flow, foam flow, annular steam flow and annular flow. They stated that as the heat load increases the flow transits from bubble–liquid slug flow to annular steam flow and then to annular flow. Gandomkar et al. [27] investigated the thermal performance and flow regimes in a ferrofluid PHP in three conditions which were the absence, presence, and elimination of the magnetic field. They used two PHPs: one made of copper and the other made of Pyrex glass. Their first observation was that the nanofluid became unstable in the copper PHP, while it preserved its stability in the Pyrex PHP. They found out that there must be an optimized concentration for the nanofluid. This is because of an increase in the shear forces with an increase in the concentration of nanofluid. However, at all concentrations, the presence of the magnetic field improved thermal performance. They observed slug–plug flow, churn flow, semi-annular flow, and annular flow in their experiments. Kang et al. [28] conducted an experiment that was similar to the work of Gandomkar et al. [27]. They reported the sedimentation of ferrofluid in Pyrex PHP in two conditions which were the absence and the presence of a magnetic field. Their PHP showed an improvement in thermal performance when the working fluid was ferrofluid particularly when the heat input was low. When the heat input was 160 W, the prevailing flow regime was annular flow and there was no difference among the thermal performance of different working fluids.

The above literature review shows that the process in which a nanofluid becomes unstable and the occurrence of aggregation of nanoparticles in a PHP need more investigations. In this study, parameters affecting the stability of nanofluid are investigated. In addition, the effect of nanofluid stability on the performance of PHP is surveyed. This includes the investigation of thermal performance and flow regimes in two PHPs. Two nanofluids are used in this study namely, graphene/water nanofluid with a high thermal conductivity and poor stability and titania/water nanofluid with a lower thermal conductivity and better stability.

## Experimental

### Experimental setup

Two PHPs were used in this research. One was made of copper and the other was made of Pyrex glass. Both the PHPs were one-turn and closed loop. The copper PHP had an inner diameter of 2 mm and an outer diameter of 4 mm, a height of 30 cm and the length of the evaporator, condenser, and adiabatic section was 8, 8, and 14 cm, respectively. The radius of the curved sections was 3 cm. To visualize the flow patterns in the copper PHP, a small piece of Pyrex glass was attached to the PHP in the adiabatic section. For sealing the space between the Pyrex glass and copper, UHU glue was used. It must be noted that flow pattern and nucleation of bubbles in the evaporator section could not be visualized in this configuration. The Pyrex PHP had an inner diameter of 3 mm and an outer diameter of 6 mm. The height of the Pyrex PHP was 28 cm and the length of the evaporator, condenser, and adiabatic section was 7, 7, and 14 cm, respectively.

To apply heat to two PHPs, nickel–chrome wire elements with an electrical resistant of  $32 \Omega \text{ m}^{-1}$  were used. Despite the fact that our working fluids had no magnetic properties, two rows of elements were wrapped around the copper and Pyrex glass PHPs to minimize the effect of any magnetic field. The elements used in the copper PHP had a coating that prevented elements from direct contact with copper. However, in the Pyrex PHP, there was no need for this coating and the wire elements were in direct contact with the glass. Heat was applied using a power supply and the boundary condition in the evaporator section was constant heat flux.

The condenser part of the copper PHP was placed in a box made of Plexiglas. The dimensions of the box were  $100 \text{ mm} \times 120 \text{ mm} \times 60 \text{ mm}$ . Cooling water with a temperature of  $18 \text{ }^\circ\text{C}$  entered from one side and exited

from the other. The cooling procedure for the Pyrex PHP was similar to the copper PHP, but the dimensions of the Plexiglas box were different from the copper PHP and were  $66 \text{ mm} \times 100 \text{ mm} \times 60 \text{ mm}$ .

For temperature measurement in the copper PHP, 4 k-type thermocouples were used. Three of them were attached to the evaporator section and the last one was attached to the condenser. Temperature data were recorded by a datalogger with a frequency of 1 Hz. For the Pyrex PHP, no thermocouple was used, because the thermal conductivity of glass was so poor that the temperature oscillations could not be recorded accurately.

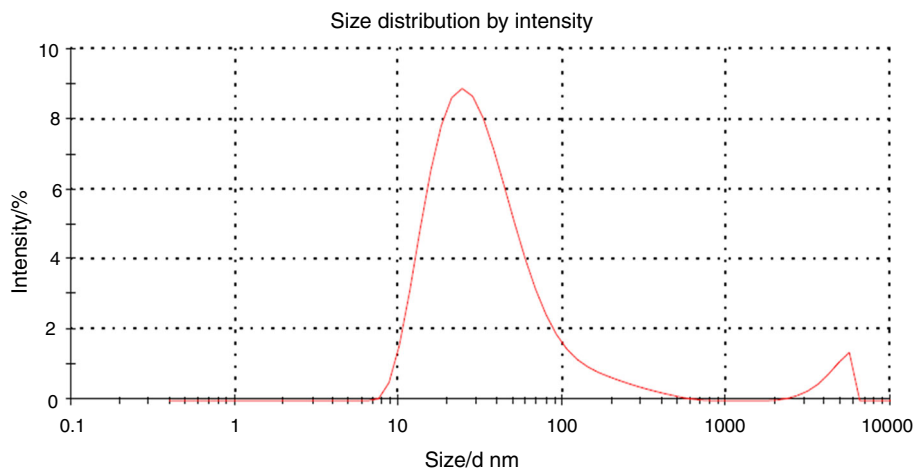
Using ceramic fiber wool, the insulation against heat was installed in the evaporator and adiabatic section of the copper PHP. For the Pyrex PHP, the insulation obstructed visualization process. Therefore, no insulating material was used for the Pyrex PHP. Without any insulating material, heat dissipation increased and the measured heat input was not the actual heat received by working fluid.

Visualization was done by a high-speed camera. The camera was connected to a PC and the pictures of the flow were recorded in real time.

### Nanofluid preparation

In this investigation, three working fluids were used: double-distilled water, titania/water nanofluid, and graphene/water nanofluid. The titania/water nanofluid was synthesized based on the work of Mohammadi et al [29]. They used a sol–gel method to prepare titania/water nanofluid. They stabilized their sol by controlling its pH value. The zeta potential of titania/water nanofluid was measured to be 27 mV that shows the good stability of this nanofluid. The concentration of the titania/water nanofluid in the current work was  $10 \text{ mg mL}^{-1}$ . Figure 1 shows the size distribution of titania nanoparticles. According to this figure, the average diameter of titania nanoparticles in the solution

**Fig. 1** Size distribution of titania nanoparticles



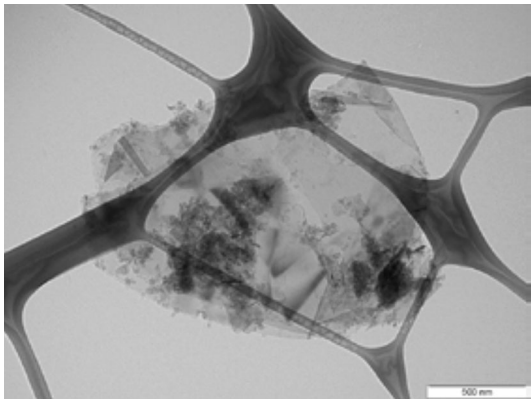


Fig. 2 TEM image of graphene nanoplatelets [30]

was 29 nm. The other nanofluid was graphene/water nanofluid. Graphene nanoplatelets were purchased from XG Sciences. They were grade C with a surface area of  $300 \text{ m}^2 \text{ g}^{-1}$ . Complete information about the graphene nanoplatelets is available in the catalogs of XG Sciences company. In Fig. 2, a TEM image of graphene nanoplatelets [30] is shown. Graphene is an inherently hydrophobic material and the stability of graphene/water nanofluid is not favorable. To disperse graphene in water, graphene powder was sonicated in water for an hour. This was performed in an ultrasonic bath. After sonication, the dispersion showed good homogeneity. The concentration of the graphene/water nanofluid was  $1 \text{ mg mL}^{-1}$ . Because of the hydrophobicity of graphene, achieving a homogenous dispersion at higher concentrations was extremely hard. The graphene/water nanofluid preserved its homogeneity and stability for several days. The zeta potential of graphene/water nanofluid was measured to be 1.54 mV that shows the poor stability of this nanofluid.

For the Pyrex PHP, no temperature was recorded and there was no reason to repeat the tests for other FRs. In fact, since Pyrex PHPs are not applicable, viable, and beneficial, it was not intended to neither improve its heat transfer performance nor compare its performance with the copper PHP. The first reason to conduct the experiments in the Pyrex PHP was to find out what is happening to a nanofluid inside a Pyrex PHP and the second reason was to find out of any difference between the flow regimes of a nanofluid PHP and a water PHP. Hence, the FR was 50% in all the experiments conducted in the Pyrex PHP. The heat input applied to the Pyrex PHP started from 5 W, and after that, 10 W was applied. After that, heat input increased with an increment of 10 W in each step. In contrast with the case of the copper PHP, heat input applied to the Pyrex PHP was not constant for a fixed time, and when all the phenomena that occurred in the Pyrex PHP was recorded by the camera, the heat input was increased. Due to temperature limit considerations, the highest power applied to the Pyrex PHP was 60 W.

### Thermal resistance and error analysis

The thermal performance of the copper PHP was evaluated by calculating the thermal resistance and heat transfer coefficient. For calculating the thermal resistance, the below equation was used:

$$R_{\text{eff}} = \frac{\bar{T}_{\text{evp}} - \bar{T}_{\text{cond}}}{Q}, \tag{1}$$

where  $\bar{T}_{\text{evp}}$ ,  $\bar{T}_{\text{cond}}$ ,  $Q$ , and  $R$  are the average temperature of the evaporator section ( $^{\circ}\text{C}$ ), the average temperature of the condenser section ( $^{\circ}\text{C}$ ), heat input applied to the PHP (W), and the thermal resistance of the PHP ( $^{\circ}\text{C W}^{-1}$ ), respectively. Error analysis for the thermal resistance was done by a technique presented by Holman and Gajda [31]. Applying this method to the current case, the below equation is obtained:

$$\frac{\delta R_{\text{eff}}}{R_{\text{eff}}} = \sqrt{\left(\frac{\delta \bar{T}_{\text{evp}}}{\bar{T}_{\text{evp}} - \bar{T}_{\text{cond}}}\right)^2 + \left(\frac{\delta \bar{T}_{\text{cond}}}{\bar{T}_{\text{evp}} - \bar{T}_{\text{cond}}}\right)^2 + \left(\frac{\delta \bar{T}_{\text{log}}}{\bar{T}_{\text{evp}} - \bar{T}_{\text{cond}}}\right)^2 + \left(\frac{\delta Q}{Q}\right)^2}, \tag{2}$$

For the copper PHP, to find the FR that PHP has the best performance in it, 3 FRs were chosen, namely, 30, 50, and 70%. The heat input increased from 10 to 70 W with an increment of 10 W in each step. The heat input in each step was constant for 30 min. During 30 min, comprehensive information about the thermal performance and flow regimes in the copper PHP was obtained.

where:

$$\begin{aligned} \left(\frac{\delta Q}{Q}\right) &= \frac{0.001}{Q} \\ \delta \bar{T}_{\text{evp}} &= \delta \bar{T}_{\text{cond}} = 0.5 \\ \delta \bar{T}_{\text{log}} &= 0.1. \end{aligned}$$

The heat transfer coefficient of PHP was calculated by the following equation:

$$h = \frac{Q}{A_{\text{evp}} \Delta T}, \quad (3)$$

where  $h$ ,  $A_{\text{evp}}$ , and  $\Delta T$  are heat transfer coefficient ( $\text{W m}^{-2} \text{ } ^\circ\text{C}^{-1}$ ), lateral surface of the evaporator ( $\text{m}^2$ ), and temperature difference between the evaporator and the condenser ( $^\circ\text{C}$ ), respectively. The lateral surface was obtained from the formula  $A_{\text{evp}} = 2\pi rL$ , where  $r$  and  $L$  are the outside radius of the pipe and the length of the evaporator section, respectively. With  $r = 2 \text{ mm}$  and  $L = 20 \text{ cm}$ , the lateral surface was calculated to be  $2.51 \times 10^{-3} \text{ m}^2$ .

Error analysis for the heat transfer coefficient was done in a similar manner to the thermal resistance. Hence, the equation for error analysis is as follows:

$$\frac{\delta h}{h} = \sqrt{\left(\frac{\delta \bar{T}_{\text{evp}}}{\bar{T}_{\text{evp}} - \bar{T}_{\text{cond}}}\right)^2 + \left(\frac{\delta \bar{T}_{\text{cond}}}{\bar{T}_{\text{evp}} - \bar{T}_{\text{cond}}}\right)^2 + \left(\frac{\delta \bar{T}_{\text{log}}}{\bar{T}_{\text{evp}} - \bar{T}_{\text{cond}}}\right)^2 + \left(\frac{\delta Q}{Q}\right)^2 + \left(\frac{\delta A}{A}\right)^2}. \quad (4)$$

Substituting values of  $\delta \bar{T}_{\text{evp}}$ ,  $\delta \bar{T}_{\text{cond}}$ ,  $\delta \bar{T}_{\text{log}}$  and  $\delta Q$  in Eqs. (2) and (4), the maximum values achieved from the tests were calculated to be 7% and 7.88% for the thermal resistance and heat transfer coefficient, respectively.

## Results and discussion

### Observations in the copper PHP

Stability of nanofluid: after decreasing the pressure inside the copper PHP by a vacuum pump, the working fluid is injected into the PHP. Because of capillary forces, the working fluid stands in the PHP in the form of liquid slugs and vapor plugs. After injection into the copper PHP, the titania/water nanofluid preserves its homogeneity and stays stable. The nanofluid is allowed to stay in the PHP for several hours without any heat applied to the PHP in this period and is then evacuated. The evacuated nanofluid maintains its stability and homogeneity, but when the heat is applied to the PHP, the acidity of the nanofluid may cause a chemical reaction between the copper wall of the PHP and the nanofluid. Therefore, the nanofluid becomes unstable and aggregations start to form. The evacuated nanofluid has a heterogeneous form and nanoparticles clusters can easily be observed. The case for graphene/water nanofluid is different. Right after the nanofluid injection, aggregation process begins and aggregated nanoparticles come down and settle on the adjacent vapor plug. Similar to the titania/

water nanofluid, the graphene/water nanofluid is allowed to stay for several hours inside the PHP and is then evacuated. The evacuated nanofluid is completely unstable and heterogeneous and graphene nanoparticles are precipitated at the bottom of the evacuated solution in the form of clusters. From these observations, it can be concluded that the material that a PHP is made of and the temperature of the working fluid are the factors that affect the stability of a nanofluid. Among these two factors, the temperature of the working fluid has the greatest effect. When the temperature increases, the collisions of the nanoparticles become more intense and it is, therefore, too difficult for a nanofluid to stay stable at high temperatures.

Flow patterns: flow regimes in the copper PHP are the same for all of working fluids. This observation is different from previous observations. As it is said, the main reason that makes the difference between the flow regimes of a

nanofluid PHP and a water PHP is the sedimentation of nanoparticles. The sedimentation changes the number of nucleation sites and the surface roughness of the wall of PHP. Hence, when the flow regimes do not change, the reason for such an observation can be that the surface roughness of the wall and the number of nucleation sites do not change. We may interpret the above-mentioned phenomena in the following four ways:

1. The size of nanoparticles is smaller than the size of the surface roughness and the sedimentation does not change the surface roughness and the number of nucleation sites.
2. Nanofluid is stable and no sedimentation occurs and hence, the surface roughness and the number of nucleation sites do not change.
3. Nanofluid concentration is not high, and therefore, the quantity of nanoparticles that precipitates is not enough to change the surface properties.
4. The surface of the wall is so smooth and the precipitation cannot change the surface roughness and the number of nucleation sites.

There is not enough information about the surface properties of the copper PHP before and after the tests, but in this study, the above-mentioned cases of 1, 2 and 3 may happen in the copper PHP.

FR and heat input are the factors affecting the flow regimes. It must be noted that the flow could only be visualized at the small piece of glass in the adiabatic section, and therefore, the flow and nucleation phenomenon in

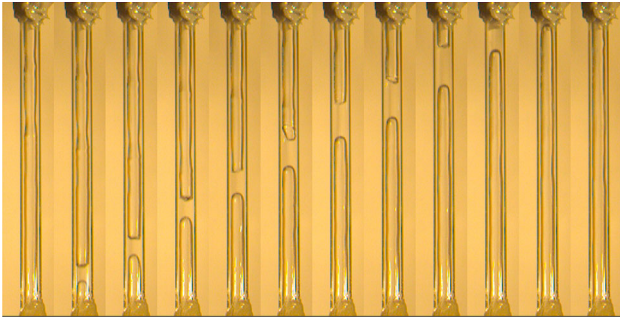


**Fig. 3** Vapor plug motion (FR = 30%, heat input = 10 W, working fluid = titania/water nanofluid with a concentration of  $10 \text{ mg mL}^{-1}$ ). The time span between each pair of adjacent images is 19 ms

the evaporator and condenser sections cannot be discussed here. In the following flow, regimes are discussed based on different FR and heat input.

For the case of 30% FR, when heat input is 10 W, the flow includes elongated vapor bubbles that oscillate between the evaporator and condenser sections and the dominant flow is annular flow. In Fig. 3, an elongated vapor plug that comes from the evaporator can be observed. The vapor plug pushes the adjacent liquid slug to the condenser. The receding head of the upper vapor plug distorts in its way to the condenser. The distortion happens because of the thin liquid film falling from the condenser section. The falling film affects the interface of the liquid and vapor plug and distorts it. When heat input increases to 20 W, dryout occurs and the temperature of the evaporator section increases inordinately.

For the case of 50% FR, the flow pattern in this FR is different from the flow pattern at 30% FR. At 10 W, the flow pattern resembles that of 30% FR, such that the dominant flow pattern at this heat input is annular flow. At 10 W, oscillating motions are not persistent and there are periods when the flow stops and there are no oscillating motions. When the flow stops, no heat is transferred and the evaporator temperature increases. Stagnation continues until the pressure difference that is necessary for the beginning of the oscillations, between the evaporator and condenser sections is reached and then intense oscillating motions begin and the temperature of the evaporator rapidly decreases. By increasing the heat input, oscillating motions and the velocity of the flow increase. These changes improve the thermal performance of the copper PHP. In Fig. 4, the distortion of the vapor plug can be observed. The flow pattern in Fig. 4 is churn–annular flow. At heat inputs of 40 or 50 W, a transition in the modes of motion occurs and the circulation of small vapor plugs and liquid slugs begins. The circulation mode has the highest efficiency among the other modes and the temperature difference between the evaporator and condenser sections

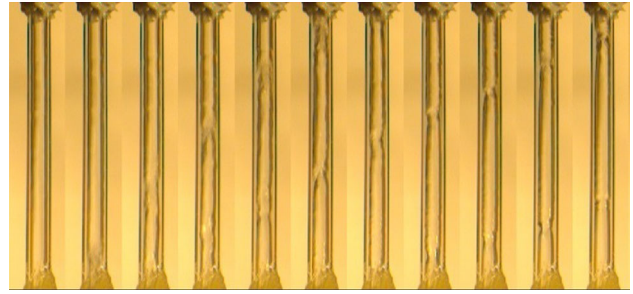


**Fig. 4** Distortion in vapor plug (FR = 50%, heat input = 40 W, working fluid = graphene/water nanofluid with a concentration of  $1 \text{ mg mL}^{-1}$ ). The time span between each pair of adjacent images is 3 ms

is  $\sim 10\text{--}15 \text{ }^\circ\text{C}$ . The circulation mode is shown in Fig. 5. In Fig. 5, the motion of small vapor plugs and bubbles from the condenser to the evaporator can be seen.

For the case of 70% FR, when heat input is 10 W, in the beginning, liquid slugs and vapor plugs move rapidly. Gradually, the flow pattern begins to switch between two flow regimes and two modes of motion. In the first case, a long vapor plug comes from the evaporator section (Fig. 6) and it goes up rapidly, but when it reaches near the condenser section, it loses its temperature and momentum and, finally, stops and then starts to go back to the evaporator section. Thus, the flow pattern is annular flow. In the other case, circulation of small liquid slugs and vapor plugs occurs. None of these flow patterns are dominant and transition between these two flow patterns causes cease in the motion of flow. Therefore, the flow pattern at 10 W is irregular and thermal performance is not desirable. At 20 and 30 W, circulation of liquid slugs and vapor plugs gradually becomes the dominant flow pattern such that an excellent thermal performance can be seen. However, long vapor plugs coming from the evaporator can be observed on several occasions. At 40 W, unlike the prior heat inputs, annular flow is the dominant flow regime, where after circulation of liquid slugs and vapor plugs for a short time

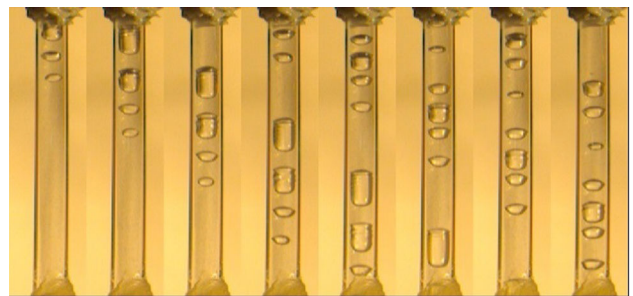


**Fig. 5** Circulation of vapor plugs and liquid slugs (FR = 50%, heat input = 70 W, working fluid = graphene/water nanofluid with a concentration of  $1 \text{ mg mL}^{-1}$ ). The time span between each pair of adjacent images is 15 ms

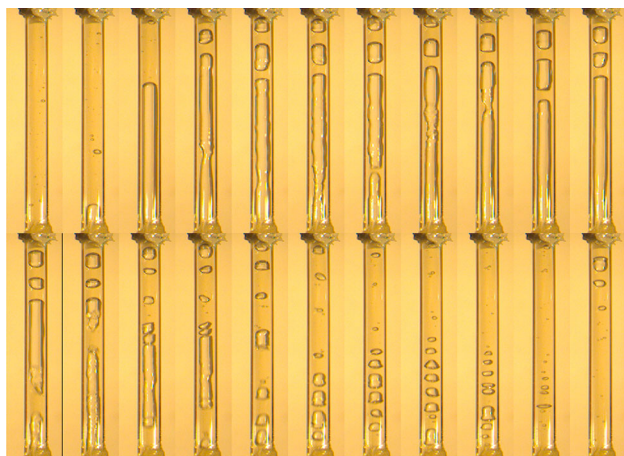


**Fig. 6** Boiling vapor plug (FR = 70%, heat input = 40 W, working fluid = titania/water nanofluid with a concentration of  $10 \text{ mg mL}^{-1}$ ). The time span between each pair of adjacent images is 15 ms

( $\sim 1\text{--}2$  min), annular flow and boiling vapor plug emerge. At 50, 60, and 70 W, the dominant mode of motion and flow pattern is the circulation of liquid slugs and vapor plugs and annular flow is not observed.

### Observations in the Pyrex PHP

Stability of nanofluid: both nanofluids keep their stability and homogeneity when injected into the Pyrex PHP even after several hours. The interesting observation is that by applying heat to the Pyrex PHP, the nanoparticles precipitate on the surface of the evaporator, but the rest of the nanofluid keeps its homogeneity. The sedimentation changes the concentration of the nanofluid. When the vapor plug is in the evaporator, the thin liquid film that comes down through the wall of PHP is in direct contact with heat and partially evaporates. After the evaporation, the nanoparticles settle on the wall of the evaporator. If the stagnation of vapor plug lasts a long time, more nanoparticles settle on the surface. At high heat inputs, there is no stagnation period, but the temperature is high and a short time is needed for evaporation of nanofluid and sedimentation of nanoparticles. This process can also occur in the copper PHP, but in the copper PHP, the stagnation period is short, and at low heat inputs, the chance of sedimentation by this process is low. A similar phenomenon was observed by Kim et al. [32] in the pool boiling process of nanofluids. They stated that in nanofluid pool boiling, a thin liquid microfilm forms underneath a nucleating vapor bubble. Microfilm evaporation causes precipitation of the nanoparticles initially contained in the nanofluid.

Flow patterns: there was no difference between the flow regimes of a nanofluid PHP and a water PHP. The possible reasons were discussed in “Observations in the copper

PHP” section. For a Pyrex PHP, the main reason must be the case 4. In addition, case 2 and 3 are probable. The surface of the Pyrex wall is so smooth and the nucleation of bubbles is not strong in the Pyrex PHP. Hence, the precipitated nanoparticles cannot change the surface roughness and the number of nucleation sites.

When heat (5 W) is applied and cooling water enters the condenser box, expansion of vapor plugs in the evaporator section begins and vapor plugs in the adiabatic section contract until an equilibrium condition is reached. Then, a stagnation period begins, where the initial distribution of vapor plugs and liquid slugs has a major effect on the distribution of vapor plugs and liquid slugs. At low heat inputs (5 and 10 W), the PHP works in a cycle that includes a stagnation period and then a period of intense oscillations. Our observations show that three conditions can occur in the stagnation period. In Condition (1), a long vapor plug completely fills the evaporator and the symmetric shape of the one-turn closed-loop PHP helps the stagnation period to stand for a long time. This is a reason PHPs with more than one turn are so desirable. In a closed-loop PHP with two or more loops, the asymmetric distribution of vapor and liquid phases and different pressure values of each turn of evaporator prevent such situations. Usually, this condition lasts  $\sim 10\text{--}15$  min. After this, the vapor plug moves from one side to the proximity of the condenser and from the other side moves to area near the curved section of the evaporator. In this way, asymmetry is created, severe oscillations begin and the vapor plug goes to the condenser and is replaced by a liquid slug. Surely, without any flow motion in this situation, no heat is transferred and temperature in the evaporator increases drastically. Another behavior in Condition (1) that is observed before severe oscillating motions is harmonic oscillations with constant amplitude. In Condition (2), two vapor plugs exist in the evaporator section and a liquid slug stands between them and separates them. Usually, in this condition, harmonic oscillations occur before severe oscillating motions. It seems that the part of heat that the liquid slug in the evaporator absorbs causes harmonic oscillations of the liquid slug. These harmonic oscillations can continue for about 5–10 min. The amplitude of harmonic oscillations is not constant, and every time, harmonic oscillations occur, and the amplitude is between 1 and 10 cm. It is obvious that these oscillating motions can transfer a part of the heat and the device in this condition has a better thermal performance than its thermal performance at low heat inputs (5 or 10 W). In Condition (3), a liquid slug fills the evaporator or at least one side and the curved section of the evaporator. Because of the large volume of liquid in the evaporator, this period may last for several minutes. In Fig. 7, an example of each condition is shown. Severe oscillations in condition (3) begin when



**Fig. 7** Three conditions that occur in the stagnation period of the Pyrex PHP at 5 and 10 W **a** condition (1): a large vapor plug completely fills the evaporator **b** condition (2): a liquid slug stands between two vapor plugs in the evaporator **c** condition (3): a liquid slug completely fills the evaporator

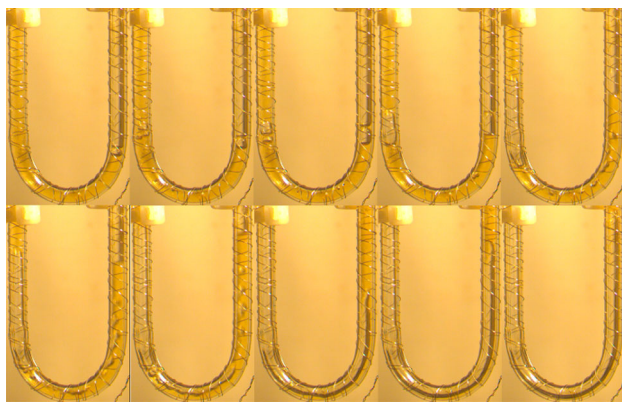
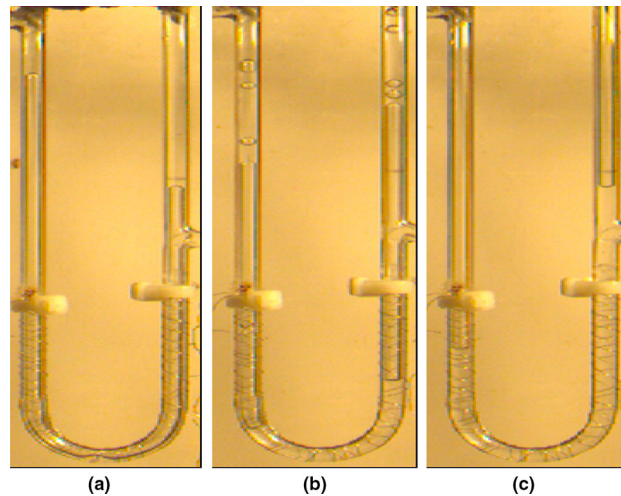


**Fig. 8** Rapid nucleation and expansion of vapor bubbles (FR = 50%, heat input = 40 W, working fluid = titania/water nanofluid with a concentration of  $10 \text{ mg mL}^{-1}$ ). The time span between each pair of adjacent images is 32 ms

rapid nucleation of a vapor bubble occurs (Fig. 8). In Fig. 8, a vapor bubble nucleates from the left side of the evaporator and expands quickly and fills the evaporator. As the heat input increases (20 W or more), oscillating motions become dominant and the stagnation period becomes shorter. The prevailing condition in the stagnation period is two vapor plugs that one extends from the curved section of the evaporator to near the condenser and the other extends from the curved section of the condenser to near the evaporator. One of these long vapor plugs stands on the right side of the PHP and the other stands in the left side. This asymmetric placement eases the initiation of

oscillating motions and after  $\sim 10\text{--}60$  s, rapid oscillations begin. However, it is possible that one of the three stagnation conditions that were described earlier occurs and thermal performance is disrupted. The last heat input applied to the PHP is 60 W. The flow pattern in this heat input is the same flow pattern as 40 and 50 W, but the difference is the faster oscillating motion and consequently better thermal performance of the PHP at this heat input.

### Thermal performance of the copper PHP

Thermal performance of the copper PHP is analyzed based on Figs. 9–13. In Figs. 9 and 10, the thermal resistance and heat transfer coefficient of the PHP at 50% FR are represented, respectively. As it is seen, at 10, 20, 30, and 40 W, the thermal resistance has its highest values for graphene/water nanofluid. The reason is that graphene nanoparticles are deposited in the PHP or aggregated in the base fluid and the thermal conductivity of the nanofluid decreases. The nanoparticles act as junk particles resulting in disruption of the flow motion and increase of thermal resistance. Another reason is that precipitated nanoparticles create a nanoparticle layer which increases the resistance to heat transfer from the wire elements to the nanofluid. The thermal resistance has its lowest values for titania/water nanofluid. This nanofluid is stable and the stability helps the nanofluid to keep its high thermal conductivity. By increasing the heat input, the difference between the thermal resistance of different working fluids decreases. When the heat input

**Fig. 9** Thermal resistance of the copper PHP with different working fluids at FR = 50%

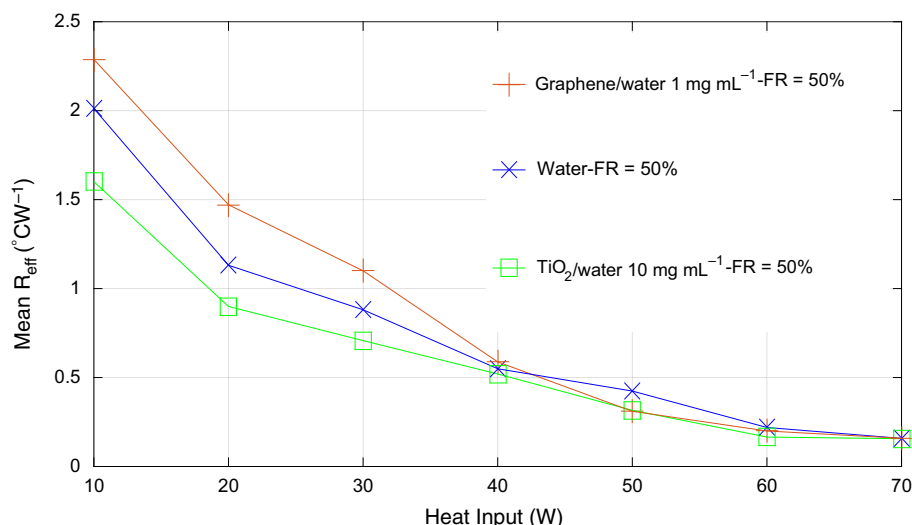
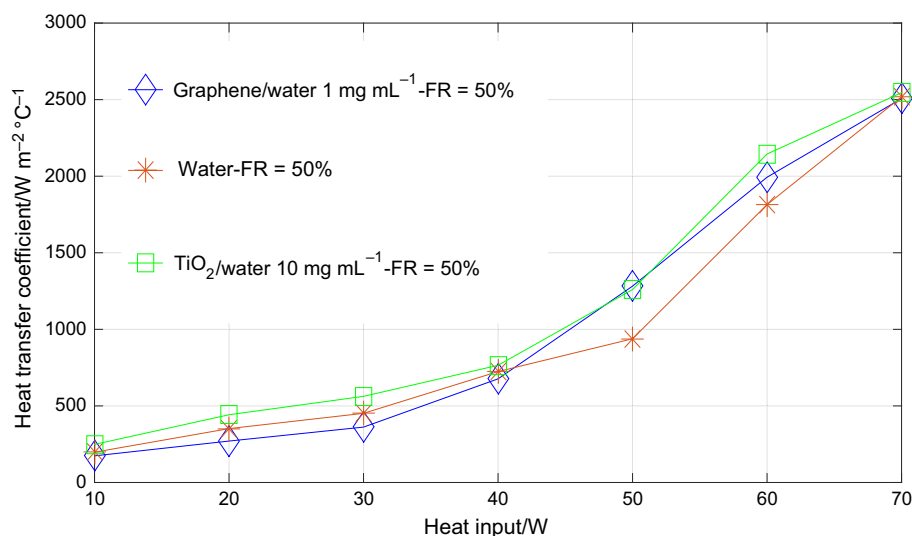


**Fig. 10** Heat transfer coefficient of the copper PHP with different working fluids at FR = 50%



increases to 60 and 70 W, the thermal resistance becomes nearly equal for all of the working fluids. Ma et al. [33] mentioned that by increasing the heat input, the oscillating motions become faster and the effect of nucleation sites decreases. Hence, the thermal performance of a nanofluid PHP and a water PHP is the same at high heat inputs. Trends for the heat transfer coefficient are similar to the thermal resistance. Graphene/water nanofluid has the lowest heat transfer coefficient and titania/water has the highest heat transfer coefficient. The lowest thermal resistance and the highest heat transfer coefficient at 50% FR are  $0.1563 \text{ }^{\circ}\text{C W}^{-1}$  and  $2546 \text{ W m}^{-2} ^{\circ}\text{C}^{-1}$ , respectively. These values belong to titania/water nanofluid that is the more stable nanofluid.

In Figs. 11 and 12, the thermal resistance and heat transfer coefficient of PHP at the 70% FR are shown, respectively. Trends in these figures are similar to the 50% FR and the more stable nanofluid has a better thermal

performance again. The lowest thermal resistance and the highest heat transfer coefficient at this FR are  $0.156 \text{ }^{\circ}\text{C W}^{-1}$  and  $2551 \text{ W m}^{-2} ^{\circ}\text{C}^{-1}$ , respectively. Again, these values were achieved for titania/water nanofluid that is the nanofluid with higher value of zeta potential.

Thermal performance at FR = 30% is only evaluated at 10 W, as was mentioned earlier. After 10 W, dry out occurs in the PHP. For water, titania/water nanofluid, and graphene/water nanofluid at FR = 30% and 10 W, the thermal resistance was 2.63, 2.094, and  $2.88 \text{ }^{\circ}\text{C W}^{-1}$  and the heat transfer coefficient was 151, 190, and  $138 \text{ W m}^{-2} ^{\circ}\text{C}^{-1}$ , respectively. These values show the better thermal performance of PHP filled with titania/water nanofluid.

To find the best FR, in Fig. 13, thermal resistance for all tests is represented. At 10 W, The lowest thermal resistance belongs to titania/water nanofluid with the

**Fig. 11** Thermal resistance of the copper PHP with different working fluids at FR = 70%

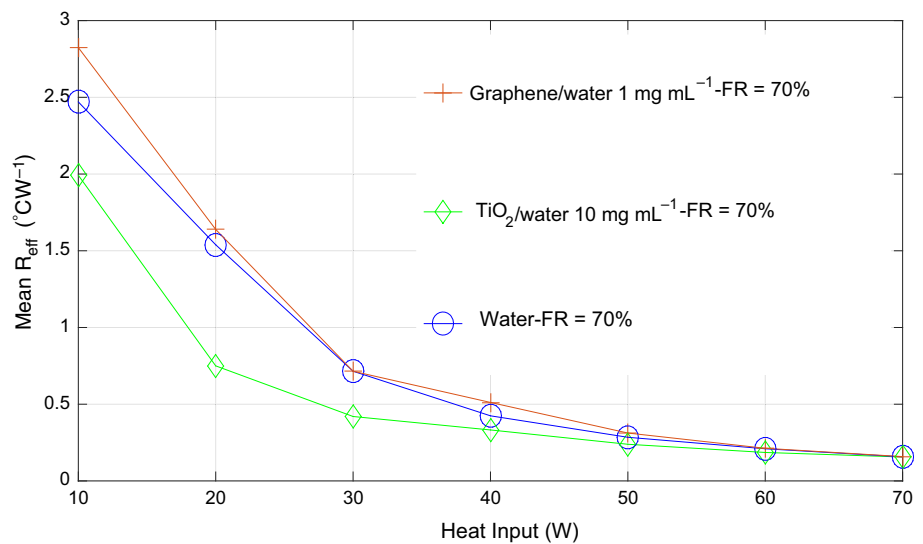
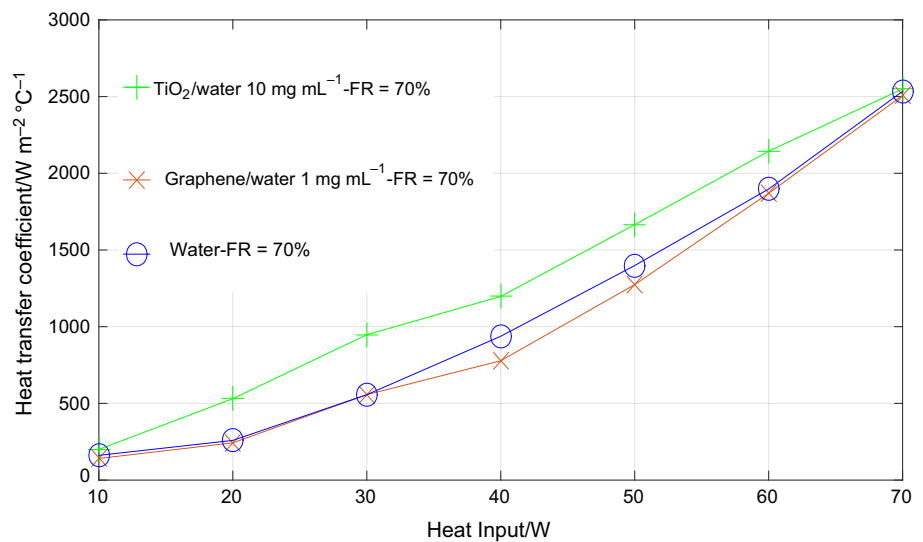


**Fig. 12** Heat transfer coefficient of the copper PHP with different working fluids at FR = 70%



concentration of 10 mg mL<sup>-1</sup> and the 50% FR. This nanofluid is stable and the stability helps the nanofluid to keep its high thermal conductivity. At this heat input, PHP has the best thermal performance at 50% FR and all working fluids have a lower thermal resistance at 50% FR than 70 and 30% FRs. At 70% FR, there is more volume of liquid than 50% FR and the energy that must be given to the working fluid to overcome the inertial force is larger than 50% FR, and therefore, at 10 W, the thermal resistance is higher at 70% FR than the 50% FR. By increasing the heat input to 20 W, the thermal resistance of the titania/water nanofluid with 70% FR reaches the lowest value among other working fluids and the thermal performance of this nanofluid is better at the 70% FR than 50% FR. However, for graphene/water nanofluid and water still the thermal performance is better at 50% FR than 70% FR. At heat inputs of 30, 40, and 50 W, the thermal performance

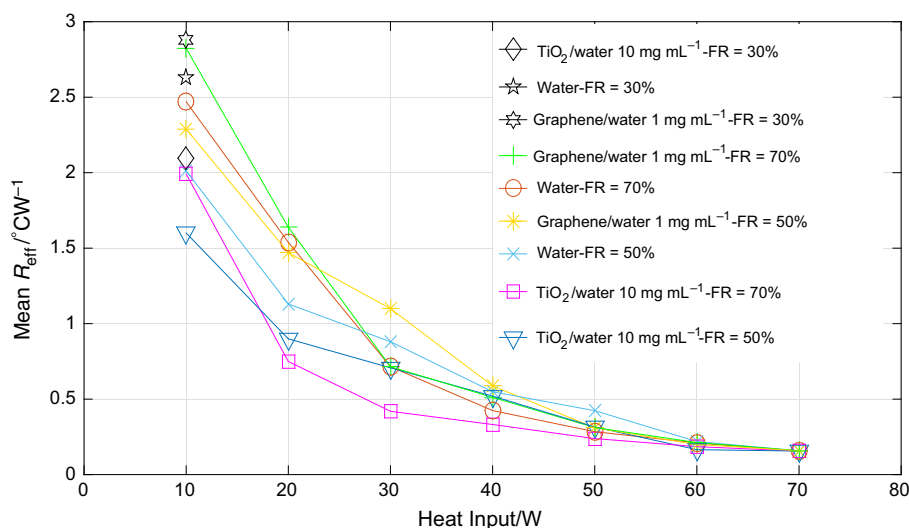
at 70% FR is better than 50% FR, but by increasing the heat input, the difference between the thermal resistance of different working fluids decreases and the thermal resistance is nearly equal for all tests at 70 W.

### Conclusions and future work

The objective of this research was to investigate the parameters affecting the stability of a nanofluid inside a PHP and to realize the effect of nanofluid stability on the thermal performance and flow patterns in a PHP. The obtained results and conclusions are as follows:

1. The material that is used to fabricate the PHP and the temperature of the working fluid are the most effective parameters on nanofluid stability. The way that is chosen to stabilize the nanofluid is also important.

**Fig. 13** Thermal resistance of the copper PHP with different working fluids at different FRs



- The less stable nanofluid easily become unstable in the copper PHP, while the more stable nanofluid preserves its stability. In the Pyrex PHP, both nanofluids keep their stability and homogeneity, but nanoparticles precipitate on the surface of the evaporator section.
- Nanofluid and its stability have no sensible effect on flow regime of PHP. The affecting parameters are FR and heat input. Precipitated nanoparticles do not change the rate of bubble nucleation in the Pyrex PHP. The reason is the smooth surface of Pyrex.
- The flow patterns which are observed in the PHPs are mainly slug flow, annular flow, bubbly flow, and churn–annular flow. Two modes of motion are observed for the motion of flow components, namely, oscillating motion and circulation. Circulation is always along with small liquid slugs, vapor plugs, and bubbles.
- Stability of nanofluid has a major effect on the thermal performance of the PHP. The more stable nanofluid has a better thermal performance than the base fluid and the less stable nanofluid has a worse thermal performance than the base fluid. The best thermal performance belongs to the 70% FR and the heat input of 70 W and was achieved for titania/water nanofluid that is the more stable nanofluid. The thermal resistance for this case is  $0.156 \text{ } ^\circ\text{C W}^{-1}$ .

There are different ways to stabilize nanofluids. Future work can be the investigation of the effect of these different ways on the performance of PHP. One of these ways is regulating the pH of nanofluid that leads to different levels of nanofluid stability. Investigation of the effect of nanofluid pH on the performance of PHP is a promising case.

**Acknowledgements** Financial support from Iran National Science Foundation (INSF), through Grant No. 940017 is greatly acknowledged.

## References

- Akachi H. Structure of a heat pipe. Google Patents; 1990.
- Nasiri H, Jamalabadi MYA, Sadeghi R, Safaei MR, Nguyen TK, Shadloo MS. A smoothed particle hydrodynamics approach for numerical simulation of nano-fluid flows. *J Therm Anal Calorim*. 2018. <https://doi.org/10.1007/s10973-018-7022-4>.
- Safaei MR, Ahmadi G, Goodarzi MS, Safdari Shadloo M, Goshayeshi HR, Dahari M. Heat transfer and pressure drop in fully developed turbulent flows of graphene nanoplatelets–silver/water nanofluids. *Fluids*. 2016;1(3):20.
- Safaei MR, Safdari Shadloo M, Goodarzi MS, Hadjadj A, Goshayeshi HR, Afrand M, Kazi S. A survey on experimental and numerical studies of convection heat transfer of nanofluids inside closed conduits. *Adv Mech Eng*. 2016;8(10):1687814016673569.
- Safaei MR, Goodarzi M, Akbari OA, Shadloo MS, Dahari M. Performance evaluation of nanofluids in an inclined ribbed microchannel for electronic cooling applications. *Electronics cooling*. InTech; 2016.
- Heydari A, Akbari OA, Safaei MR, Derakhshani M, Alrashed AA, Mashayekhi R, Shabani GAS, Zarringhalam M, Nguyen TK. The effect of attack angle of triangular ribs on heat transfer of nanofluids in a microchannel. *J Therm Anal Calorim*. 2018;131(3):2893–912.
- Safaei MR, Mahian O, Garoosi F, Hooman K, Karimipour A, Kazi S, Gharekhani S. Investigation of micro- and nanoparticle erosion in a 90 pipe bend using a two-phase discrete phase model. *Sci World J*. 2014;2014:30–41.
- Karimipour A, Esfe MH, Safaei MR, Semiromi DT, Jafari S, Kazi S. Mixed convection of copper–water nanofluid in a shallow inclined lid driven cavity using the lattice Boltzmann method. *Physica A Stat Mech Appl*. 2014;402:150–68.
- Karimipour A, Nezhad AH, D’Orazio A, Esfe MH, Safaei MR, Shirani E. Simulation of copper–water nanofluid in a microchannel in slip flow regime using the lattice Boltzmann method. *Eur J Mech-B/Fluids*. 2015;49:89–99.
- Raei B, Shahraki F, Jamialahmadi M, Peyghambarzadeh S. Experimental study on the heat transfer and flow properties of γ-

- Al<sub>2</sub>O<sub>3</sub>/water nanofluid in a double-tube heat exchanger. *J Therm Anal Calorim.* 2017;127(3):2561–75.
11. Stalin PMJ, Arjunan T, Matheswaran M, Sadanandam N. Experimental and theoretical investigation on the effects of lower concentration CeO<sub>2</sub>/water nanofluid in flat-plate solar collector. *J Therm Anal Calorim.* 1–16.
  12. Riehl RR, dos Santos N. Water-copper nanofluid application in an open loop pulsating heat pipe. *Appl Therm Eng.* 2012;42:6–10.
  13. Zhao N, Zhao D, Ma H. Experimental investigation of magnetic field effect on the magnetic nanofluid oscillating heat pipe. *J Therm Sci Eng Appl.* 2013;5(1):011005.
  14. Mohammadi M, Taslimifar M, Saidi MH, Shafii MB, Afshin H, Hannani SK. Ferrofluidic open loop pulsating heat pipes: efficient candidates for thermal management of electronics. *Exp Heat Transf.* 2014;27(3):296–312.
  15. Goshayeshi H, Goodarzi M, Dahari M. Effect of magnetic field on the heat transfer rate of kerosene/Fe<sub>2</sub>O<sub>3</sub> nanofluid in a copper oscillating heat pipe. *Exp Therm Fluid Sci.* 2015;68:663–8.
  16. Goshayeshi HR, Goodarzi M, Safaei MR, Dahari M. Experimental study on the effect of inclination angle on heat transfer enhancement of a ferrofluid in a closed loop oscillating heat pipe under magnetic field. *Exp Therm Fluid Sci.* 2016;74:265–70.
  17. Goshayeshi HR, Safaei MR, Goodarzi M, Dahari M. Particle size and type effects on heat transfer enhancement of Ferro-nanofluids in a pulsating heat pipe. *Powder Technol.* 2016;301:1218–26.
  18. Lin YH, Kang SW, Chen HL. Effect of silver nano-fluid on pulsating heat pipe thermal performance. *Appl Therm Eng.* 2008;28(11):1312–7.
  19. Qu J, Wu H. Thermal performance comparison of oscillating heat pipes with SiO<sub>2</sub>/water and Al<sub>2</sub>O<sub>3</sub>/water nanofluids. *Int J Therm Sci.* 2011;50(10):1954–62.
  20. Ji Y, Liu G, Ma H, Li G, Sun Y. An experimental investigation of heat transfer performance in a polydimethylsiloxane (PDMS) oscillating heat pipe. *Appl Therm Eng.* 2013;61(2):690–7.
  21. Das SK, Putra N, Thiesen P, Roetzel W. Temperature dependence of thermal conductivity enhancement for nanofluids. *J Heat Transf.* 2003;125(4):567–74.
  22. Esfe MH, Yan WM, Akbari M, Karimipour A, Hassani M. Experimental study on thermal conductivity of DWCNT-ZnO/water-EG nanofluids. *Int Commun Heat Mass Transf.* 2015;68:248–51.
  23. Wilson C, Borgmeyer B, Winholtz R, Ma H, Jacobson D, Hussey D, Arif M. Visual observation of oscillating heat pipes using neutron radiography. *J Thermophys Heat Transf.* 2008;22(3):366–72.
  24. Bhuwaktikumjohn N, Rittidech S. Internal flow patterns on heat transfer characteristics of a closed-loop oscillating heat-pipe with check valves using ethanol and a silver nano-ethanol mixture. *Exp Therm Fluid Sci.* 2010;34(8):1000–7.
  25. Li QM, Zou J, Yang Z, Duan YY, Wang BX. Visualization of two-phase flows in nanofluid oscillating heat pipes. *J Heat Transf.* 2011;133(5):052901.
  26. Goshayeshi HR, Chaer I. Experimental study and flow visualization of Fe<sub>2</sub>O<sub>3</sub>/kerosene in glass oscillating heat pipes. *Appl Therm Eng.* 2016;103:1213–8.
  27. Gandomkar A, Saidi MH, Shafii M, Vandadi M, Kalan K. Visualization and comparative investigations of pulsating ferrofluid heat pipe. *Appl Therm Eng.* 2017;116:56–65.
  28. Kang SW, Wang YC, Liu YC, Lo HM. Visualization and thermal resistance measurements for a magnetic nanofluid pulsating heat pipe. *Appl Therm Eng.* 2017;126:1044–50.
  29. Mohammadi M, Fray D, Mohammadi A. Sol-gel nanostructured titanium dioxide: controlling the crystal structure, crystallite size, phase transformation, packing and ordering. *Microporous Mesoporous Mater.* 2008;112(1):392–402.
  30. <https://xgsciences.com/wp-content/uploads/2017/11/xGnP-C.-MD00001.-2018-1.pdf>.
  31. Holman JP, Gajda WJ. *Experimental methods for engineers.* New York: McGraw-Hill; 2004.
  32. Kim SJ, Bang IC, Buongiorno J, Hu L. Surface wettability change during pool boiling of nanofluids and its effect on critical heat flux. *Int J Heat Mass Transf.* 2007;50(19):4105–16.
  33. Ma H, Wilson C, Yu Q, Park K, Choi U, Tirumala M. An experimental investigation of heat transport capability in a nanofluid oscillating heat pipe. *J Heat Transf.* 2006;128(11):1213–6.